

Convective and Diffusive Energetic Particle Losses Induced by Shear Alfvén Waves in the ASDEX Upgrade Tokamak

M. García-Muñoz,^{1,*} N. Hicks,¹ R. van Voornveld,² I. G. J. Classen,^{1,2} R. Bilato,¹ V. Bobkov,¹ M. Bruedgam,¹ H.-U. Fahrback,¹ V. Igochine,¹ S. Jaemsae,³ M. Maraschek,¹ K. Sassenberg,¹ and ASDEX Upgrade Team

¹Max-Planck-Institut für Plasmaphysik, EURATOM Association Boltzmannstraße 2, D-85748 Garching, Germany

²FOM-Institute for Plasma Physics Rijnhuizen, Association EURATOM-FOM, P.O. Box 1207, 3430 BE Nieuwegein, The Netherlands

³Helsinki University of Technology, Association Euratom-Tekes, P.O. Box 4100, FIN-02015 HUT, Finland

(Received 28 December 2009; published 6 May 2010)

We present here the first phase-space characterization of convective and diffusive energetic particle losses induced by shear Alfvén waves in a magnetically confined fusion plasma. While single toroidal Alfvén eigenmodes (TAE) and Alfvén cascades (AC) eject resonant fast ions in a convective process, an overlapping of AC and TAE spatial structures leads to a large fast-ion diffusion and loss. Diffusive fast-ion losses have been observed with a single TAE above a certain threshold in the fluctuation amplitude.

DOI: 10.1103/PhysRevLett.104.185002

PACS numbers: 52.55.Pi, 52.35.Bj

Alfvén waves are ubiquitous in astrophysical as well as in laboratory plasmas [1]. Their interplay with energetic ions is of crucial importance to understanding the energy and particle exchange in astrophysical plasmas [2] as well as to obtaining a viable energy source in magnetically confined fusion devices such as ITER [3]. In astrophysics, Alfvénic instabilities are thought to be responsible for the anomalous transport of particles and energy in regimes such as the heating of the solar corona or the generation of the solar wind [4–7]. In magnetically confined fusion plasmas, the excitation of shear Alfvén waves such as reverse shear Alfvén eigenmodes (RSAEs) [8,9], so-called Alfvén cascades (ACs), and toroidal Alfvén eigenmodes (TAEs) [10,11] is of special importance for addressing the fast-ion transport across the magnetic field lines because of their potential to eject fast ions before their thermalization [12,13].

The nonlinear evolution of Alfvénic instabilities driven by energetic particles and the subsequent redistribution of those particles has been the focus of exhaustive theoretical studies [14–19]. A wave-particle exchange of momentum and energy takes place in tokamaks if the resonant condition $\Omega_{n,p} = n\omega_\phi - p\omega_\theta - \omega \approx 0$ is fulfilled [20]. Here, n is the toroidal mode number, p is the poloidal harmonic, ω_ϕ the fast-ion precession frequency, ω_θ the fast-ion poloidal frequency, ω the mode frequency and $\Omega_{n,p}$ the resonance width [21,22]. At each resonance, the wave-particle momentum exchange, proportional to the fluctuation amplitude δB , corresponds to a radial drift of the fast ions. This linear momentum exchange may cause convective losses of fast ions if the right wave-particle relative phase is given. However, depending on whether modes spatial structures and phase-space resonances overlap local or global redistribution of fast ions may occur [23]. If most of the relevant phase space is covered by overlapping resonances particles can be lost via stochastic diffusion [24]. For single modes, stochastic losses caused by the overlapping of sideband resonances are proportional

to $(\delta B)^2$ [15]. Experimentally, a detailed knowledge of the wave-particle interaction can be gained from direct measurements of MHD induced fast-ion losses in fusion plasmas [25,26]. Fast-ion loss detectors (FILD) in fusion devices obtain typically a crucial information on the phase space of the lost ions [27–31].

In this Letter, we present the phase-space characterization of convective and diffusive fast-ion losses induced by shear Alfvén waves in a magnetically confined fusion plasma. The experiments discussed here have been performed in plasmas with toroidal plasma current $I_p \approx 0.8$ MA, toroidal field $B_t = 2.0$ T, safety factor at the edge $q_{95} \approx 4.0$, and ion cyclotron resonance heating (ICRH) as the main heating and fast particle source. 4.5 MW of on axis ICRH hydrogen minority heating was applied to a deuterium plasma ($n_H/n_D \approx 5\%$). Figure 1(a) shows the core line integrated electron density, n_e , and neutron rate for the discharge presented here, #23824. Figures 1(b) and 1(c) show, respectively, the Fourier spectrogram for a magnetic fluctuation signal and for a soft x-ray (SXR) signal, corresponding to a line of sight passing through the plasma core. Several coherent MHD fluctuations are visible around 110 kHz up to 170 kHz. They correspond to TAEs with different toroidal mode numbers [32] n 's ($n = 3, 4, 5$), as obtained from Mirnov coils [33], whose identification is confirmed also by comparison with ideal MHD calculations carried out with the CASTOR code [34]. Magnetic fluctuations chirping up in frequency from ≈ 50 kHz up to the TAE frequencies, $f_{\text{TAE}} = V_A/4\pi q R_0$, are barely visible in the magnetics spectrogram. Here, V_A is the Alfvén speed and R_0 is the major radius. These frequency chirping fluctuations have been identified as ACs by means of the SXR emission from the plasma core as Fig. 1(c) shows. The lowest AC frequency, $f_{\text{AC}}^{\text{min}}$, in Fig. 1 is mainly given by the geodesic compressibility and the toroidal coupling to the acoustic waves, as expected by the theory [35]. Pressure effects modify the local dispersion relation for shear Alfvén waves in low- β plas-

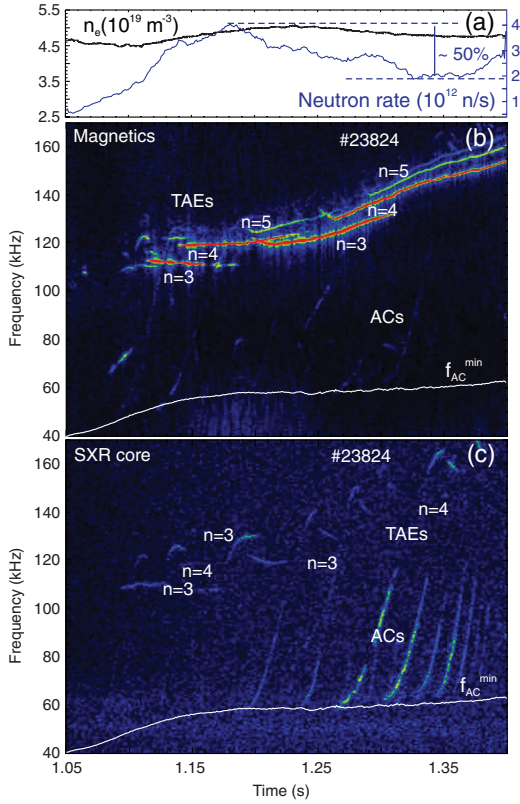


FIG. 1 (color). AUG discharge #23824: (a) core line integrated electron density n_e and neutron rate. (b) Spectrogram of an invessel magnetic pickup coil. (c) Spectrogram of a core SXR channel, the lowest AC frequency, f_{AC}^{\min} , is superimposed in white.

mas: $\omega_{AC} \approx \left| \frac{m}{q_{\min-n}} \right| \frac{V_A}{R_0}$, with m the poloidal mode number. The modified minimum of the local dispersion relation is then given by

$$\omega_{AC}^{\min} \approx \frac{\sqrt{2}}{R_0} C_s = \frac{\sqrt{2}}{R_0} \left(\frac{T_i}{m_i} \right)^{1/2} \left(\frac{7}{4} + \frac{T_e}{T_i} \right)^{1/2}. \quad (1)$$

An excellent agreement between the experimental lowest AC frequency and the modified dispersion relation given in Eq. (1) is clearly visible. The estimated f_{AC}^{\min} has been calculated assuming $T_e = T_i$ and taking T_e from an electron cyclotron emission (ECE) radiometer channel near the AC localization. The neutron rate in Fig. 1(a) shows a drop of $\approx 50\%$ in the presence of strong TAEs and ACs, indicating a redistribution of fast deuterium ions created by high harmonic ICRH.

Fluctuations in the electron temperature profile caused by the ACs and TAEs [36] have been measured with the ECE radiometer at high resolution in space (≈ 1 cm) and time (1 MHz sampling rate). The AC and TAE radial structures have been reconstructed by means of ECE-FILD cross-correlation techniques. Figure 2 shows the normalized cross power spectral densities (coherence) as a function of ρ_{pol} and frequency for 50 ms time intervals. The AC and TAE radial structures were obtained by selecting and averaging a certain frequency band of the coher-

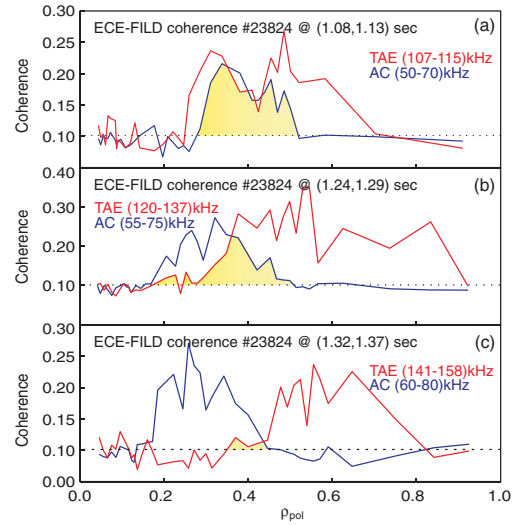


FIG. 2 (color). AUG discharge #23824: ACs and TAEs radial structures obtained by means of ECE-FILD cross correlation. AC radial structures are reconstructed at the AC lowest frequency. Different time intervals are displayed. (a) for (1.08–1.13) sec; (b) for (1.24–1.29) sec; and (c) for (1.32, 1.37) sec. The yellow areas highlight the regions with overlapping TAE-AC internal structures well before the AC-TAE transition.

ence. The selected AC and TAE frequency bands are given in Fig. 2. Figure 2(a) shows global TAEs extended from $\rho_{\text{pol}} \approx 0.23$ up to the edge with broad ACs localized at $\rho_{\text{pol}} \approx 0.4$. A complete overlapping of AC-TAE radial structures is clearly visible. Figure 2(b) shows the AC-TAE radial structures for a later time interval. TAEs shift outwards becoming more localized while ACs shift inwards becoming also more localized at $\rho_{\text{pol}} \approx 0.3$. The overlapping region (highlighted in yellow) becomes smaller. Finally, Fig. 2(c) shows a neglectable AC-TAE spatial overlapping with ACs and TAEs well localized at $\rho_{\text{pol}} \approx 0.3$ and $\rho_{\text{pol}} \approx 0.6$, respectively. The largest ACs and TAEs presented here caused a normalized T_e perturbation of $\delta T_e/T_e \approx 0.009$.

In order to fully characterize the orbits of the lost ions and identify the wave-particle resonances responsible for the losses, the phase-space (energy and pitch angle) of the fast-ion losses is shown in Fig. 3. In the presence of multiple AEs, e.g., $t = 1.36$ s, fast ions are ejected within a broad energy range with a gyroradius from ≈ 35 mm up to ≈ 105 mm, see Fig. 3(a). For the magnetic field at the probe, ≈ 1.6 T, this gyroradius range corresponds to hydrogen ions with energies between ≈ 0.2 and ≈ 1.4 MeV. As expected from ICRH heated plasmas the fast-ion losses appear at high pitch angles between 67° and 80° . The phase space of lost fast ions changes strongly during the evolution of the AE activity, showing a completely different pattern within the next 200 ms. Figure 3(b) presents fast-ion losses well localized at high pitch angles ($\approx 71^\circ$) and energies (gyroradius ≈ 60 mm).

A Fourier analysis of the fast-ion loss signal allows us to identify the MHD fluctuations responsible for these losses.

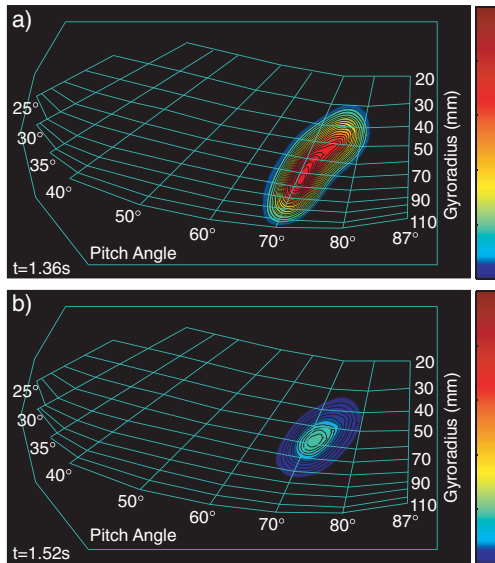


FIG. 3 (color). AUG discharge #23824: CCD frames showing the light patterns produced by ACs and TAEs induced fast-ion losses in particle phase space. (a) Fast-ion losses at $t = 1.36$ s. (b) Fast-ion losses at $t = 1.52$ s.

Figure 4(a) shows this exercise. The AC-TAE details of the FILD spectrogram are striking. A clear correlation between the TAE frequency pattern and the fast-ion loss frequencies is observed in both magnetics, Fig. 1(b), and FILD, Fig. 4(a), spectrograms. Although all TAEs eject resonant ions, the relative amplitude of the measured losses with respect to the fluctuation amplitude does not depend only on the magnetic fluctuation amplitude; e.g., the losses measured at the $n = 4$ TAE frequency are not as strong as one could expect from its large fluctuation amplitude in Fig. 1(b). Changes in the spatial distribution of the losses could explain this observation as the measurements are performed at a single poloidal position. In addition, fast-ion losses chirping in frequency from approximately the geodesic frequency f_{AC}^{\min} up to the TAE frequency f_{TAE} emerge following the typical AC frequency pattern. The AC induced resonant losses appear stronger ($\approx 10\%$ of the total resonant losses) in the frequency range where the ACs interact with the Alfvén-acoustic branch near the f_{AC}^{\min} and during the AC-TAE transition.

The raw data of the Fourier-analyzed fast-ion loss signal shown in Fig. 4(a) are presented in Fig. 4(b) to investigate the diffusive and convective character of the losses. The signal consists of a modulated (coherent) signal sitting on an incoherent background whose amplitude varies with time. The coherent component of the fast-ion losses is correlated in frequency and phase with the corresponding magnetic fluctuation, giving rise to the spectrogram shown in Fig. 4(a). The incoherent component is dominant, up to 80% of the total losses, in the presence of multiple frequency chirping AEs, $t \approx (1.1-1.3)$ s, and decreases when the number of modes decreases. However, it should be noted that it is not zero when only one mode is ejecting

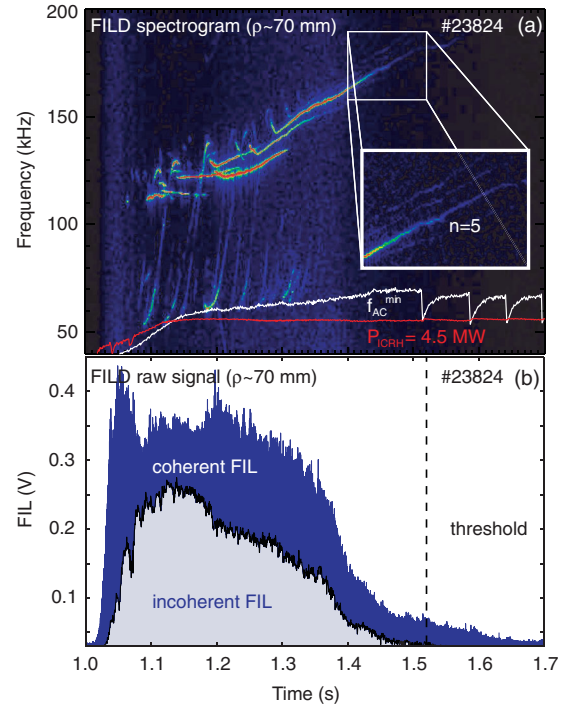


FIG. 4 (color). AUG discharge #23824. (a) spectrogram of the fast-ion loss signal with gyroradius ≈ 70 mm. The lowest AC frequency f_{AC}^{\min} is superimposed in white while the total ICRH power (P_{ICRH}) is superimposed in red. The inset shows the single TAE responsible for the onset of the incoherent losses. (b) Fast-ion loss signal. The coherent and incoherent components of the losses are highlighted. The vertical dashed line depicts the threshold for the incoherent losses.

ions with a relatively large amplitude, $t \approx (1.42-1.52)$ s, as discussed later. During the time window $t \approx (1.52-1.7)$ s only coherent losses induced by a single TAE, $n = 5$, are visible. Going backwards in time, the incoherent losses of ions with gyroradius $\approx 60-70$ mm appear, for $t \leq 1.52$ s, when the local maximum radial displacement of the magnetic field lines is larger than ≈ 2 mm as measured by its fluctuation induced on the SXR emission. This threshold in the fluctuation amplitude is depicted in Fig. 4(b) with a vertical dashed line. The basic properties of the coherent and incoherent losses are investigated through their dependence on the magnetic fluctuation amplitude. Tracking the frequencies of the individual fluctuations in both magnetics and FILD spectrograms, we get the relationship between the coherent fast-ion losses and the corresponding magnetic fluctuation amplitude. Figure 5(a) shows this exercise for the TAE $n = 3$ between $t = 1.24$ s and $t = 1.32$ s. A clear linear dependence is visible during the whole time window, showing the convective character of the underlying loss mechanism. A similar analysis has been done for the incoherent losses shown in Fig. 4(b). The envelope of the incoherent losses, black curve in Fig. 4(b), is plotted in Fig. 5(b) as a function of the amplitude of the TAE $n = 5$ for a time interval close to the onset of the incoherent losses, inset in Fig. 5(b),

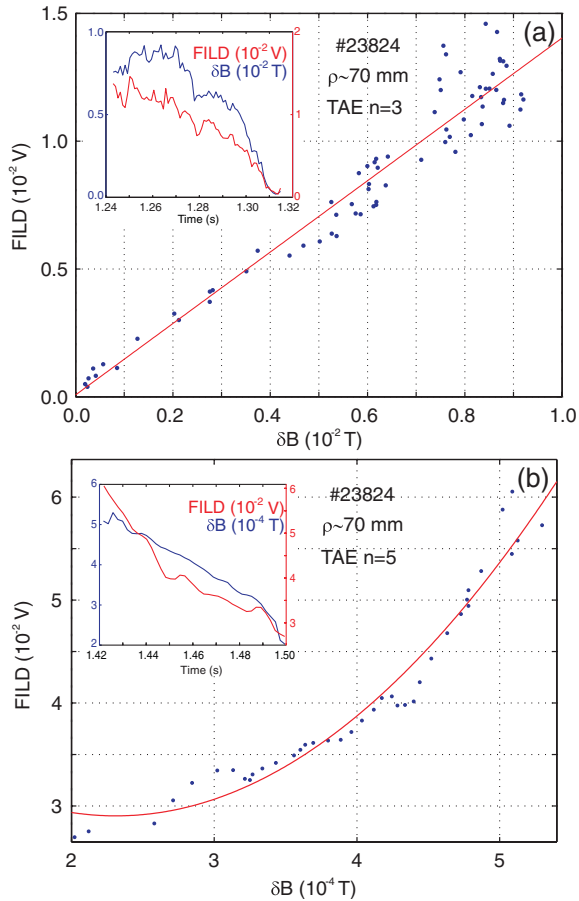


FIG. 5 (color). AUG discharge #23824: Fast-ion loss rate. (a) Linear dependence of the coherent losses at the TAE $n = 3$ frequency on the MHD fluctuation amplitude. (b) Quadratic dependence of the incoherent losses on the TAE $n = 5$ fluctuation amplitude.

$t = (1.42, 1.50)$ s. A clear quadratic dependence has been obtained, strongly suggesting a diffusive mechanism involving several resonances in phase space. This is supported by the data shown in Fig. 3(a) which indicate that the losses cover a larger domain in phase space when the incoherent signal is not zero. It should also be underlined that, as shown in Fig. 4(b), the incoherent component is even larger in the presence of several modes, which is also expected to induce a diffusive fast-ion transport.

In summary, we have characterized the phase space of convective and diffusive energetic particle losses induced by shear Alfvén waves in a magnetically confined fusion plasma. Time-resolved energy and pitch angle measurements of fast-ion losses correlated in frequency and phase with ACs and TAEs have allowed us to identify both loss mechanisms. Single ACs and TAEs eject resonant fast ions in a convective process directly proportional to the fluctuation amplitude, δB . The overlapping of multiple AC and TAE spatial structures leads to a large diffusive loss. Since these structures propagate in the plasma with differ-

ent phase velocities, a simple explanation in terms of stochasticization in real space cannot be given. It remains a subject of further studies to explain how incoherent losses can occur under these conditions. For single TAEs, diffusive losses of fast ions, scaling as $(\delta B)^2$, are observed for local radial displacements of the magnetic field lines larger than ≈ 2 mm. The results presented here may be of general interest for better understanding the wave-particle interactions and subsequent energy and particle transport in fusion devices as well as in astrophysical plasmas.

The authors wish to thank H.L. Berk, F. Ryter, and H. Zohm for very fruitful discussions.

*Manuel.Garcia-Munoz@ipp.mpg.de

- [1] H. Alfvén, *Nature (London)* **150**, 405 (1942).
- [2] E. Marsch, *Living Rev. Solar Phys.* **3**, 1 (2006).
- [3] M. Shimada *et al.*, *Nucl. Fusion* **47**, S1 (2007).
- [4] J. A. Miller and D. A. Roberts, *Astrophys. J.* **452**, 912 (1995).
- [5] S. R. Cranmer and A. A. van Ballegooijen, *Astrophys. J.* **594**, 573 (2003).
- [6] J. W. Cirtain *et al.*, *Science* **318** 1580 (2007).
- [7] J. A. Araneda *et al.*, *Phys. Rev. Lett.* **102**, 175001 (2009).
- [8] H. L. Berk *et al.*, *Phys. Rev. Lett.* **87**, 185002 (2001).
- [9] S. E. Sharapov *et al.*, *Phys. Lett. A* **289**, 127 (2001).
- [10] K. L. Wong *et al.*, *Phys. Rev. Lett.* **66**, 1874 (1991).
- [11] W. W. Heidbrink, *Nucl. Fusion* **31**, 1635 (1991).
- [12] W. W. Heidbrink *et al.*, *Phys. Rev. Lett.* **99**, 245002 (2007).
- [13] A. Fasoli *et al.*, *Nucl. Fusion* **47** S264 (2007).
- [14] H. L. Berk *et al.*, *Phys. Rev. Lett.* **68**, 3563 (1992).
- [15] D. Sigmar *et al.*, *Phys. Fluids B* **4**, 1506 (1992).
- [16] H. E. Mynick, *Phys. Fluids B* **5**, 1471 (1993).
- [17] B. N. Breizman *et al.*, *Phys. Fluids B* **5**, 3217 (1993).
- [18] Y. Todo *et al.*, *Phys. Plasmas* **10**, 2888 (2003).
- [19] G. Vlad *et al.*, *Nucl. Fusion* **49**, 075024 (2009).
- [20] R. B. White *et al.*, *Phys. Fluids* **26**, 2958 (1983).
- [21] H. L. Berk *et al.*, *Nucl. Fusion* **35** 1661 (1995).
- [22] S. D. Pinches *et al.*, *Nucl. Fusion* **46**, S904 (2006).
- [23] H. L. Berk *et al.*, *Phys. Plasmas* **2** 3007 (1995).
- [24] B. V. Chirikov, *Phys. Rep.* **52**, 263 (1979).
- [25] W. W. Heidbrink *et al.*, *Phys. Rev. Lett.* **53**, 1905 (1984).
- [26] K. Nagaoka *et al.*, *Phys. Rev. Lett.* **100**, 065005 (2008).
- [27] S. J. Zweben *et al.*, *Nucl. Fusion* **39**, 1097 (1999).
- [28] M. Isobe *et al.*, *Nucl. Fusion* **46**, S918 (2006).
- [29] D. Darrow *et al.*, *Nucl. Fusion* **48**, 084004 (2008).
- [30] M. Garcia-Munoz *et al.*, *Phys. Rev. Lett.* **100**, 055005 (2008).
- [31] M. Garcia-Munoz *et al.*, *Rev. Sci. Instrum.* **80**, 053503 (2009).
- [32] J. A. Wesson, *Tokamaks* (Clarendon Press, Oxford, 1997).
- [33] M. Schittenhelm, *Nucl. Fusion* **37**, 1255 (1997).
- [34] W. Kerner, *J. Comput. Phys.* **142**, 271 (1998).
- [35] B. N. Breizman *et al.*, *Phys. Plasmas* **12**, 112506 (2005).
- [36] M. A. Van-Zeeland *et al.*, *Phys. Rev. Lett.* **97** 135001 (2006).